Transition Metal Chemistry (2018) 43:563–570
https://doi.org/10.1007/s11243-018-0242-4

Synthesis, structures and characterization of two cobalt(II) coordination polymers with 2,5-dichloroterephthalic acid and flexible bis(benzimidazole) ligands

Wen-Chao Kang[1] · Yue-Hua Li[1] · Zhan-Bin Qin[1] · Guang-Hua Cui[1]

Received: 2 March 2018 / Accepted: 30 April 2018 / Published online: 25 May 2018

Abstract
Two Co(II) coordination polymers (CPs), namely $[Co(L1)(DCTP)]_n$ (**1**) and $[Co(L2)(DCTP)]_n$ (**2**) [L1 = 1,4-bis(5,6-dimethylbenzimidazol-1-yl)butane, L2 = 1,5-bis(5,6-dimethylbenzimidazol-1-yl)pentane, H_2DCTP = 2,5-dichloroterephthalic acid] were synthesized and characterized by single-crystal X-ray diffraction analysis, elemental analysis, powder X-ray diffraction (PXRD) and infrared spectroscopy. CP **1** has a 2D (4,4) corrugated sheet structure, which is further extended into a 2D double layer by C–H···O weak hydrogen bonding interactions, while CP **2** displays a 2D layer with **hcb** network, which is assembled into a 3D supramolecular framework through C–H···O hydrogen bonding. Both CPs exhibited promising photocatalytic activities for the degradation of methylene blue under UV irradiation. In addition, the thermal stabilities and the luminescence properties of both CPs have been investigated.

Introduction

The self-assembly of coordination polymers (CPs) has emerged as an important research topic in recent years, not only because of their interesting and diverse topologies, but also due to their extensive applications in catalysis, electrochemistry, gas adsorption and magnetic materials [1–7]. The final architectures of new CPs remain hard to predict because of the many factors which can influence the self-assembly process, including temperature, solvent, pH value and choice of organic ligands [8–13]. Clearly, however, one of the most important factors in obtaining a desired molecular architecture is the careful selection of organic ligands as bridging or terminal groups, with transition metals as nodes [14–18]. Recently, flexible bis(benzimidazole) derivatives, which have remarkable coordination ability and versatile conformations, have attracted much interest as N-donor ligands. They can adopt diverse conformations by means of the torsional flexibility of their $–(CH_2)_n–$ spacers, providing opportunities to meet different requirements of the metal centers in the assembly process [19, 20]. In addition, various weak intermolecular interactions may play a crucial role in the construction of supramolecular architectures with functional properties, such as hydrogen bonds and π–π stacking [21, 22]. Meanwhile, aromatic dicarboxylic acid ligands have also been widely used to synthesize coordination polymers, because of their versatile coordination modes and structural rigidity, chemical stability and appropriate connectivity [23, 24]. However, only a few metal–organic coordination polymers based on 2,5-dichloroterephthalic acid (H_2DCTP) as a bridging ligand have been successfully prepared [25, 26].

In this work, we synthesized two CPs with flexible bis(benzimidazole) and 2,5-dichloroterephthalic acid ligands (scheme 1), namely, $[Co(L1)(DCTP)]_n$ (1), and $[Co(L2)(DCTP)]_n$ (2) (L1 = 1,4-bis(5,6-dimethylbenzimidazol-1-yl)butane, L2 = 1,5-bis(5,6-dimethylbenzimidazol-1-yl)pentane). CP **1** exhibits a 2D double-layer structure, while CP **2** has a 3D supramolecular framework. The photocatalytic activities of both CPs for the degradation of methylene blue (MB) were investigated.

✉ Guang-Hua Cui
tscghua@126.com

[1] College of Chemical Engineering, Hebei Key Laboratory for Environment Photocatalytic and Electrocatalytic Materials, North China University of Science and Technology, No. 21 Bohai Road, Caofeidian new-city, Tangshan 063210, Hebei, People's Republic of China

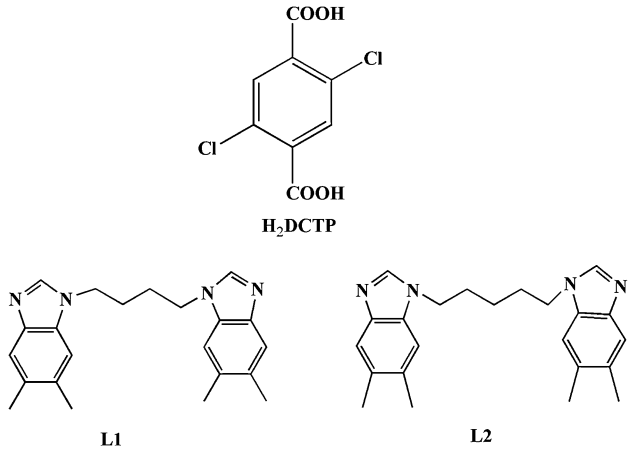

Scheme 1 Structural formulas of all ligands

Experimental

Materials and methods

The proligands L1 and L2 were synthesized according to the literature [27]. All other chemicals and reagents were purchased from Beijing InnoChem Science & Technology Co. and used without further purification. C, N and H contents were determined with a Perkin-Elmer 240C analyzer. FTIR spectra were recorded from KBr pellets in the range of 4000–400 cm^{-1} with an Avatar 360 (Nicolet) spectrophotometer. Powder X-ray diffraction (PXRD) investigations were carried out with a Rigaku D/Max-2500 diffractometer using Cu-$K\alpha$ radiation ($\lambda = 1.5418$ Å) over the 2θ range from 5 to 50° at room temperature, using 40 mA and 40 kV. An Edinburgh instruments FS5 spectrophotometer was employed to record the spectra of powdered solid samples. Thermogravimetric analyses (TGA) were recorded on a NETZSCH STA 449F3 differential thermal analyzer at a rate of 10 °C/min, under an N_2 atmosphere. Solid state UV/vis diffuse reflectance spectra were recorded on a UV–Vis spectrophotometer (Puxi, TU-1901), with a $BaSO_4$ plate as the standard at room temperature.

Synthesis of $[Co(L1)(DCTP)]_n$ (1)

A mixture of $Co(OAc)_2{\cdot}4H_2O$ (49.8 mg, 0.2 mmol), L1 (34.6 mg, 0.1 mmol), H_2DCTP (23.5 mg, 0.1 mmol), NaOH (8 mg, 0.2 mmol) and H_2O (10 mL) was sealed in a 25-mL Teflon-lined autoclave and heated continuously at 140 °C for 3 days under autogenous pressure. After cooling to room temperature at a rate of 5 °C/h, purple block-shaped crystals were obtained with 47.3% yield (based on Co). Anal. Calc. for $C_{30}H_{28}Cl_2CoN_4O_4$: C 56.4; H 4.4; N 8.8%. Found: C 56.6; H 4.1; N 8.6%. IR (cm^{-1}, KBr): 1631 (s), 1589 (s), 1511 (m), 1474 (m), 1376 (s), 1298 (w), 1076 (m), 842 (m), 524 (w).

Synthesis of $[Co(L2)(DCTP)]_n$ (2)

CP **2** was prepared by a procedure similar to CP **1**, except that L1 was replaced with L2 (36.0 mg). Purple block crystals were obtained with 43.5% yield (based on Co). Anal. Calc. for $C_{31}H_{30}Cl_2CoN_4O_4$: C, 57.1; H, 4.4; N, 8.3%. Found: C, 56.9; H, 4.6; N, 8.6%. IR (cm^{-1}, KBr): 1617 (s), 1458 (m), 1377 (s), 1307 (m), 1217 (m), 1078 (m), 829 (w), 626 (w).

X-ray crystallography

Crystallographic data for a single crystal of CP **1** were collected at 100(2) K on an Agilent Technology SuperNova Atlas Dual System with a Cu microfocus source ($\lambda = 1.54184$ Å) and focusing multilayer optics. Data for CP **2** were collected on a Bruker Smart 1000 CCD area-detector diffractometer at 296(2) K using graphite-monochromated Mo-Kα radiation ($\lambda = 0.71073$ Å) with ω scan mode. Both structures were solved by direct methods and refined with full-matrix least-squares techniques based on F^2 using the SHELXL-2014/7 program for CP **1** and SHELXL-2016/6 program for CP **2** [28]. All the non-hydrogen atoms were treated anisotropically. Hydrogen atoms of organic ligands were generated geometrically and refined isotropically using the riding model. The crystallographic data for CPs **1** and **2** are summarized in Table 1, and selected bond lengths and angles are listed in Table 2.

Photocatalytic experiments

The photocatalytic activities of CP **1** and CP **2** were evaluated for degradation of MB. Experiments were carried out under irradiation with a 500W high pressure halogen lamp. Before the reaction, 30 mg of the solid sample was added into a tube containing 100 mL of MB solution (10 mg/L). The reaction was stirred in a dark environment for 1 h in order to eliminate adsorption effects between the catalyst and solution. The solution was then exposed to UV irradiation. During the irradiation period, 3.5-mL aliquots were removed at 15-min intervals, and the liquid was separated by centrifugation. The resulting solutions were analyzed with a UV/vis spectrophotometer, to quantify the remaining MB in solution. A blank experiment was carried out under the same conditions, but without the catalyst. Considering the initial absorbance values of the dye solution as A_0, and the absorbance values at time t as A_t, the degradation efficiency (D) of the dye is defined as follows:

$$D = \left[\left(A_0 - A_t\right)/A_0\right] \times 100\%$$

Table 1 Crystal and refinement data for CPs **1**–**2**

CP	**1**	**2**
Empirical formula	C30 H28 Cl2 Co N4 O4	C31 H30 Cl2 Co N4 O4
Formula	638.39	652.42
Temperature/K	100 (2)	296 (2)
Wavelength/Å	1.54184	0.71073
Crystal system	Triclinic	Triclinic
Space group	$P\bar{1}$	$P\bar{1}$
a/Å	10.7890 (7)	9.9271 (5)
b/Å	11.1244 (4)	11.7087 (5)
c/Å	13.2776 (5)	12.7687 (6)
α/°	114.466 (4)	86.3490 (10)
β/°	97.738 (3)	75.8300 (10)
γ/°	98.349 (4)	82.3750 (10)
Volume/Å^3	1401.16 (12)	1425.52 (12)
Z	2	2
D(calc)/mg m^{-3}	1.513	1.520
Absorption coefficient/mm^{-1}	6.923	0.835
F(000)	658	674
Crystal size/mm	0.23× 0.22× 0.19	0.27× 0.26× 0.21
θ range/°	3.746–73.838	2.922–28.355
Limiting indices	$-13 \le h \le 12$ $-8 \le k \le 13$ $-16 \le l \le 16$	$-13 \le h \le 13$ $-15 \le k \le 15$ $-13 \le l \le 17$
Reflections collected	10,478	21,378
Independent reflections (R_{int})	5478/0.0445	7100/0.0333
Data/restraint/parameters	5478/0/374	7100/0/383
Goodness of fit on *F*	1.030	1.036
Final *R*, wR2 [$I > 2\sigma(I)$]	0.0561, 0.1438	0.0403, 0.0821
R (all data)[a)]	$R1 = 0.0561$, $wR2 = 0.1438$	$R1 = 0.0671$ $wR2 = 0.0897$
Largest diff. peak and hole	1.038, −0.718	0.274, −0.286

Table 2 Selected bond lengths (Å) and angles (°) for CPs **1** and **2**

CP 1			
Co(1)–O(2)	1.986(2)	Co(1)–O(3)	2.007(2)
Co(1)–N(1)	2.030(3)	Co(1)–N(4)C	2.029(3)
O(2)–Co(1)–O(3)	111.35(10)	O(3)–Co(1)–N(4)C	115.11(11)
O(2)–Co(1)–N(4)C	103.35(11)	O(2)–Co(1)–N(1)	91.88(11)
N(1)–Co(1)–O3	119.46(10)	O(4)–Co(1)–O(3)	169.078(9)
CP **2**			
Co(1)–O(1)	1.9607(15)	Co(1)–N(1)	2.0216(16)
Co(1)–O(3)	1.9676(15)	Co(1)–N(4)A	2.0506(16)
O(1)–Co(1)–N(4)A	118.36(7)	O(1)–Co(1)–O(3)	100.77(7)
O(3)–Co(1)–N(4)A	100.26(6)	O(1)–Co(1)–N(1)	114.99(7)
N(1)–Co(1)–N(4)A	103.97(7)	O(3)–Co(1)–N(1)	118.27(7)
O(3)–Co(1)–O(2)	144.58(4)		

Symmetry codes for 1: *C*: $x, y, z+1$; for 2: *A*: $-x+2, -y+1, -z+1$

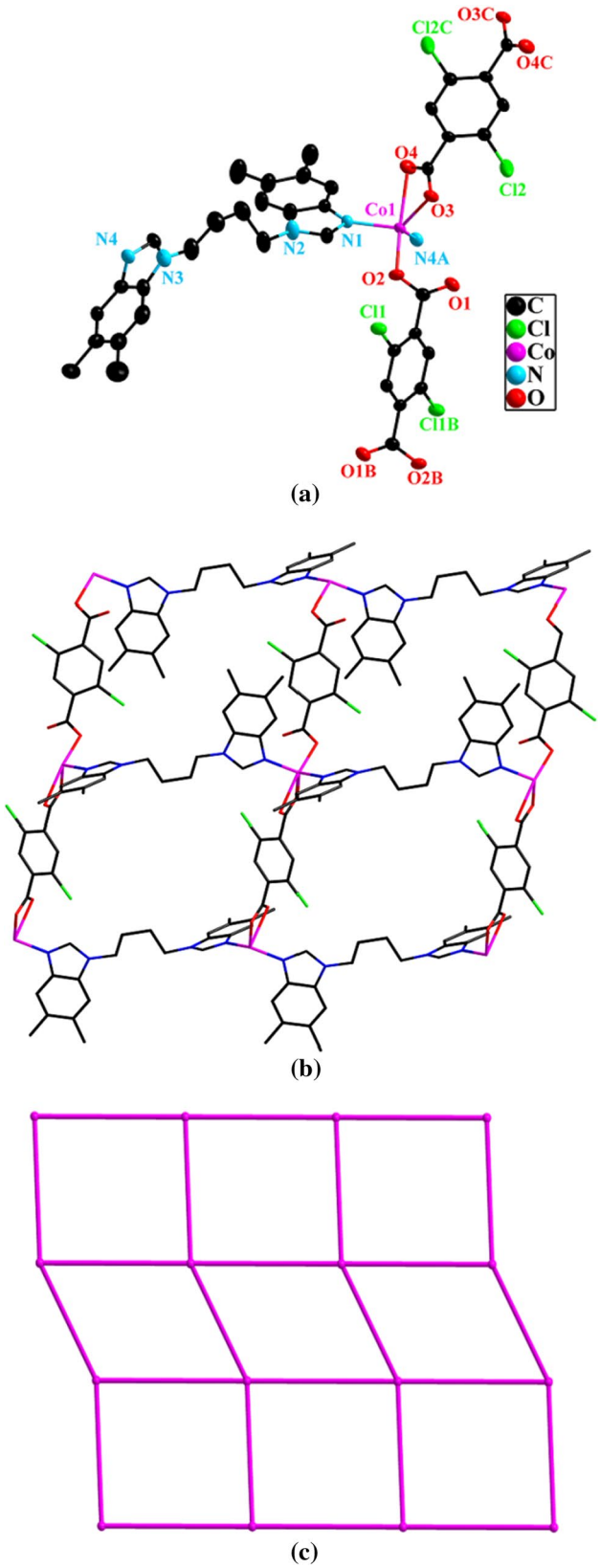

Fig. 1 **a** Coordination environment around the Co(II) centers in CP **1**. ▶ Hydrogen atoms are omitted for clarity (symmetry code: *A*: *x*, *y*, 1 + *z*, *B*: −x, −y 1 − *z*, *C*: *x*, *y*, 1 + *z*). **b** Schematic view of 2D layer constructed by ligands $DCTP^{2-}$, L1, and Co(II) centers. **c** The schematic of the 2D layer topology in CP **1**

Results and discussion

Crystal structure of CP 1

Single-crystal X-ray diffraction analysis revealed that CP **1** crystallizes in the triclinic space group *P*ī. The asymmetric unit contains one cobalt(II) center, one L1 ligand and two halves of $DCTP^{2-}$ ligands (Fig. 1a). Each Co(II) center is penta-coordinated by two nitrogen atoms (N1, N4A), (symmetry code: $A = x, y, z + 1$) from two different L1 ligands, plus three oxygen atoms (O2, O3, O4) from two $DCTP^{2-}$ ligands, assembling a slightly distorted trigonal bipyramid [CoN_2O_3] with a value of $\tau_5 = 0.82$ [29]. The Co–N bond lengths are 2.030(3) Å (Co–N1) and 2.029(3) Å (Co–N4A), and the Co–O bond lengths are 1.986(2) Å (Co–O2), 2.007(2) Å (Co–O3) and 2.448(2) Å. All these bond lengths are within the expected ranges [30].

In CP **1**, the $DCTP^{2-}$ ligands adopt alternating $(\kappa^1-\kappa^0)-(\kappa^1-\kappa^0)-\mu_2$ and $(\kappa^1-\kappa^1)-(\kappa^1-\kappa^1)-\mu_2$ coordination modes, forming a 1D straight $[Co–DCTP–Co]_n$ chain with a contiguous Co···Co distance of 10.867(9) Å. The ligand L1 shows a *trans*-coordinated conformation in which the nitrogen atoms from two benzimidazole rings concatenate neighboring Co(II) centers to build a 1D $[Co\text{-}L1\text{-}Co]_n$ straight chain. The dihedral angle between the two benzimidazole rings within a complete L1 ligand is 82.34(1), and the neighboring Co···Co distance is 13.278(1) Å. These chains are further connected by sharing of the Co(II) centers along different directions to form a 2D (4,4) network. This arrangement gives rise to a tetranuclear unit, constructed from two L1 ligands, two $DCTP^{2-}$ ligands and four Co(II) centers (Fig. 1b). The network consists of rhombuses, which can be regard as a four-connected **sql** corrugated network; the size of each rhomboid, defined by Co–Co distances, is 13.277 × 10.860 Å (Fig. 1c). The sheet structure is further developed into a 2D double layer through hydrogen bonding between C–H groups of the L1 ligands and oxygen atoms of the $DCTP^{2-}$ ligands [C10–H10A···O3, C12–H12A···O1] with H···O distances of 2.490(2) and 2.448(3) Å, respectively.

Crystal Structure of CP 2

CP **2** crystallizes in the triclinic space group *P*ī. The unit cell contains one cobalt(II) center, one L2 ligand and two halves

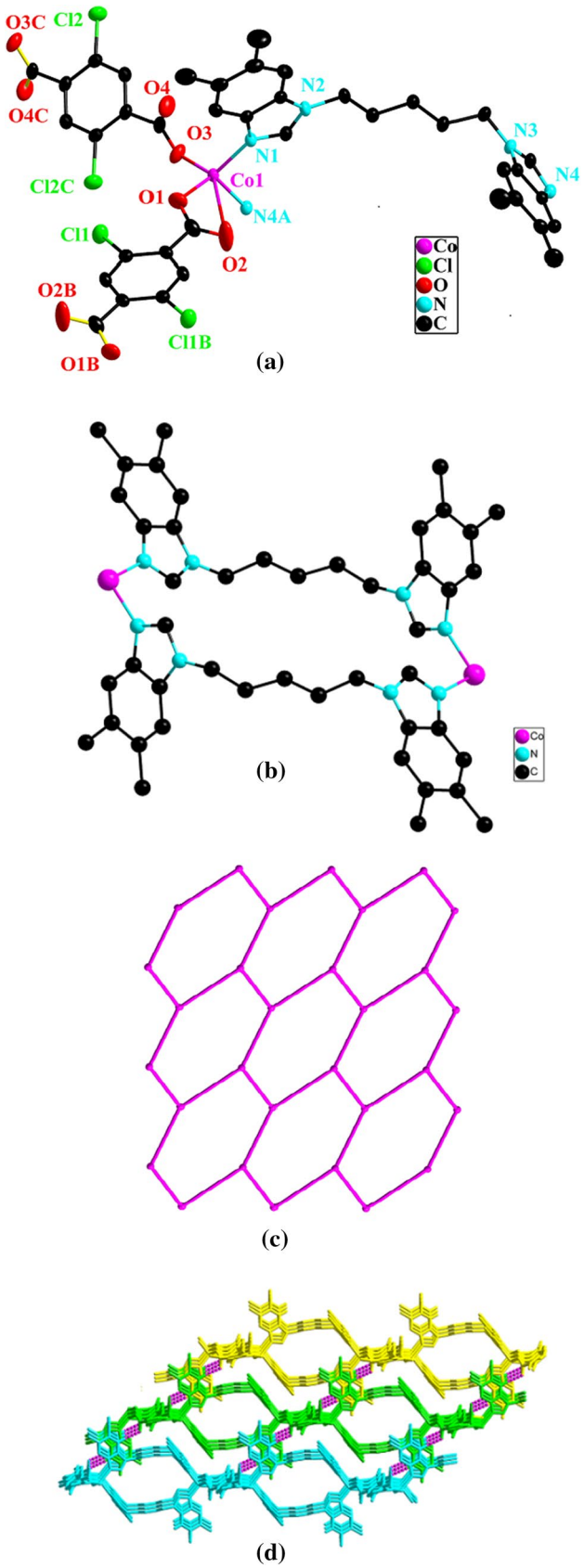

Fig. 2 **a** Coordination environment around the Co(II) centers in CP **2**. ▶ Hydrogen atoms are omitted for clarity (symmetry code: *A*: −x+2, −y+1, −z+1, *B*: −x, −y+1, −z+1, *C*: −x, −y+2, −z+2). **b** A $[Co_2(L2)_2]$ unit in CP **2**. **c** Schematic view of 2D layer constructed by ligands $DCTP^{2-}$, L2, and Co(II) centers. **d** Schematic view of the 3D supramolecular framework by C–H···O stacking interactions in CP **2**

of $DCTP^{2-}$ ligands in the asymmetric unit (as shown in Fig. 2a). The Co(II) center is penta-coordinated by two nitrogen atoms (N1, N4A), (symmetry code: $A = 2-x, -y+1, -z+1$) from two L2 ligands, plus three oxygen atoms (O1, O2, O3) from two $DCTP^{2-}$ ligands, again giving a distorted trigonal bipyramid $[CoN_2O_3]$, for which $\tau_5 = 0.43$ [29]. The Co–N bond lengths are 2.021(2) and 2.050(2) Å, while the Co–O bond lengths are in the range of 1.960 (2) to 2.854(2) Å. These values are all in the normal ranges, and comparable to those found in CP **1**.

In CP **2,** two L2 ligands are located on both sides of two Co(II) centers, adopting a bis(monodentate) coordination mode to bridge adjacent Co(II) centers in a 24-membered macrocycle $[Co_2(L2)_2]$ (Fig. 2b). The dihedral angle between the two benzimidazole rings of each L2 ligand is 88.57(7). Meanwhile, the $DCTP^{2-}$ ligands also adopt the alternating $(\kappa^1-\kappa^0)-(\kappa^1-\kappa^0)-\mu_2$ and $(\kappa^1-\kappa^1)-(\kappa^1-\kappa^1)-\mu_2$ coordinating mode seen in CP **1**, forming a 1D wave-like [Co-DCTP-Co] chain with the Co···Co distances of 11.165(6) and 11.103(5) Å. In this way, the $[Co_2(L2)_2]$ units lie on the crests and troughs of the 1D [Co-DCTP-Co] chains, such that Co···Co is 13.080(7) Å, forming a 2D layered **hcb** structure with the 3-connect point symbol $\{6^3\}$ (Fig. 2c). The 2D **hcb** layers are further connected by C–H···O hydrogen bonds, with C16–H16···O4 angle of 150° and H16···O4 distance of 2.56 Å, leading to a 3D supramolecular framework (Fig. 2d).

Influence of the N-donor ligands on the structures

In this work, we selected the carboxylic acid H_2DCTP^- and two alternative bis(benzimidazole) ligands to synthesize cobalt(II) CPs. From the structure descriptions above, ligands L1 and L2, which have different spacer lengths, act as linkers to connect the Co(II) centers in CPs **1** and **2**. The $DCTP^{2-}$ ligands in both CPs also act as linkers; they are fully deprotonated and adopt the same bis(monodentate) and bis(chelating) coordination modes. In CP **1**, the L1 ligands adopt a *trans*-coordinated mode to connect Co(II) centers, to give infinite 1D $[Co(L1)]_n$ chains which are further assembled with $DCTP^{2-}$ ligands, ultimately giving a 2D (4,4) layer structure. In CP 2, the L2 ligands again adopt a *trans*-coordinated mode to connect neighboring Co(II) centers, with a 24-membered macrocycle $[Co_2(L2)_2]$ which is further connected by $DCTP^{2-}$ ligands give a 2D (6,3) layered structure. Consequently, the spacer lengths of the bis(benzimidazole)

ligands have a significant influence on the structures of the resulting ternary Co(II) CPs.

Spectroscopic and PXRD characterization

The asymmetric and symmetric carboxylate vibrations of $DCTP^{2-}$ ligands in both CPs are evident as strong bonds at 1589, 1474 and 1376 cm^{-1} for CP **1** and at 1617, 1458 and 1377 cm^{-1} for CP **2**. The values of $\Delta\nu[\nu_{as}(COO)–\nu_{s}(COO)]$ are thus 115 and 213 cm^{-1} for CP **1** and 159 and 240 cm^{-1} for CP **2,** indicative of both the monodentate and chelating coordination modes of the $DCTP^{2-}$ ligands in CPs **1** and **2**. Bands in the region of 1500 cm^{-1} for both CPs are assigned to C=N stretching vibrations of the N-donor ligands, while bands around 640 nm^{-1} can be attributed to the C–Cl group of the $DCTP^{2-}$ ligands in both CPs.

In order to confirm the purities of both CPs, their PXRD patterns were checked at room temperature. The peak positions obtained from experiment were almost identical to the simulated PXRD crystal data (Fig. 3), confirming the phase purities of both bulk samples.

The solid state photoluminescence properties of these CPs were investigated at room temperature. The H_2DCTP ligand has a negligible contribution to the luminescence emission. Therefore, the emission of the title CPs is mainly associated with the presence of the bis(benzimidazole) ligands. The free N-donor proligands exhibit maxima at 313 nm (λ_{ex} = 280 nm) for L1 and 361 nm (λ_{ex} = 216 nm) for L2, while emission bands are observed at 522 nm (λ_{ex} = 498 nm) for CP **1** and 364 nm (λ_{ex} = 354 nm) for CP **2** (Fig. 4). Hence, compared with the free N-containing proligands, the emission peaks of both CPs are both blue-shifted, which may be due to the fact that the coordinated ligands are not allowed to relax by torsional modes on photoexcitation [31].

The absorption features of the CPs were revealed through their diffuse reflectance UV/Vis spectra (Fig. 5a). The main absorption peaks at 251 nm for CP **1** and 267 nm for CP **2** can be assigned to π*–π transitions of the ligand and/or ligand-to-metal charge transfer (LMCT) [32]. An additional absorption broad observed in the visible for CP **1,** from 526 to 592 nm, and for CP **2** from 528 to 589 nm, could originate from $d \rightarrow d$ spin-allowed transitions of the metal centers [33]. The band gap energies (E_g) of the CPs can be calculated by extrapolation of the linear portion of the absorption edges, giving values of 3.09 eV for CP **1** and 3.58 eV for CP **2** (Fig. 5b) according to the formula. The energy band gap sizes suggest that these CPs may exhibit potential capability for photocatalytic degradation under UV irradiation. Where R is the reflectance at a given energy, the formula is as follows:

$$F(R) = (1 - R)^2/2R$$

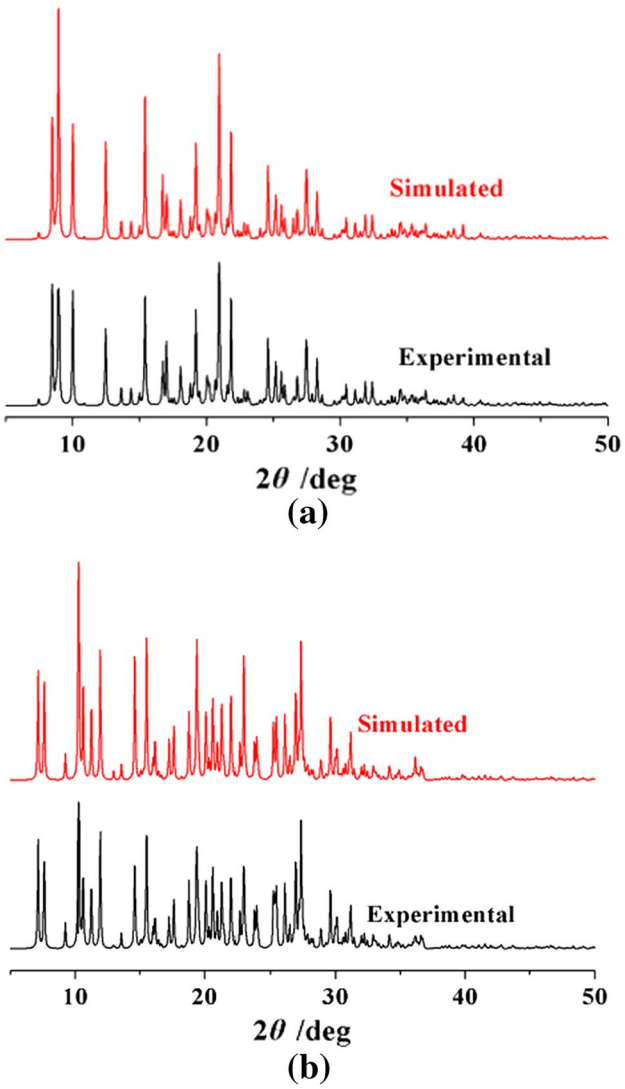

Fig. 3 Simulated and experimental patterns of X-ray powder diffraction of CP **1** (**a**) and CP **2** (**b**)

Thermogravimetric analysis

In order to assess the thermodynamic stabilities of these CPs, TGA experiments were carried out (Fig. 6). For CP **1,** there is one weight loss in the temperature range from 290 to 590 °C, attributed to the decomposition of all organic ligands. The residue is identified as CoO (calcd. 11.7%, found. 12.1%). The thermogravimetric analysis of CP **2** showed one weight loss stage between 280 and 550 °C, again assigned to decomposition of all organic ligands. The residue is again CoO (calcd. 11.5%, found. 11.7%).

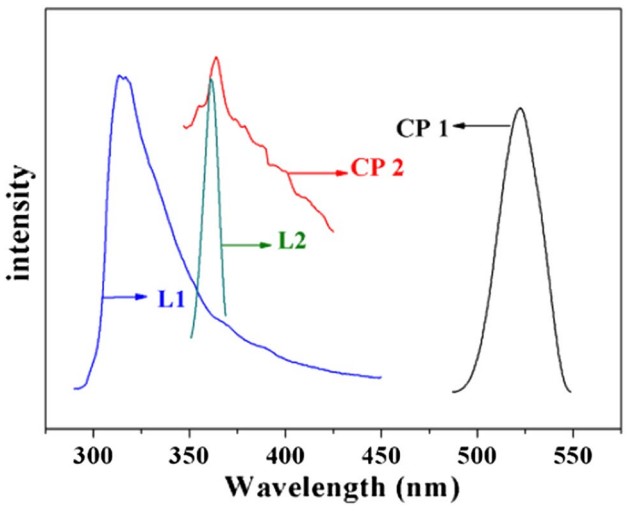

Fig. 4 Emission spectra of CPs **1**–**2** and the free ligands

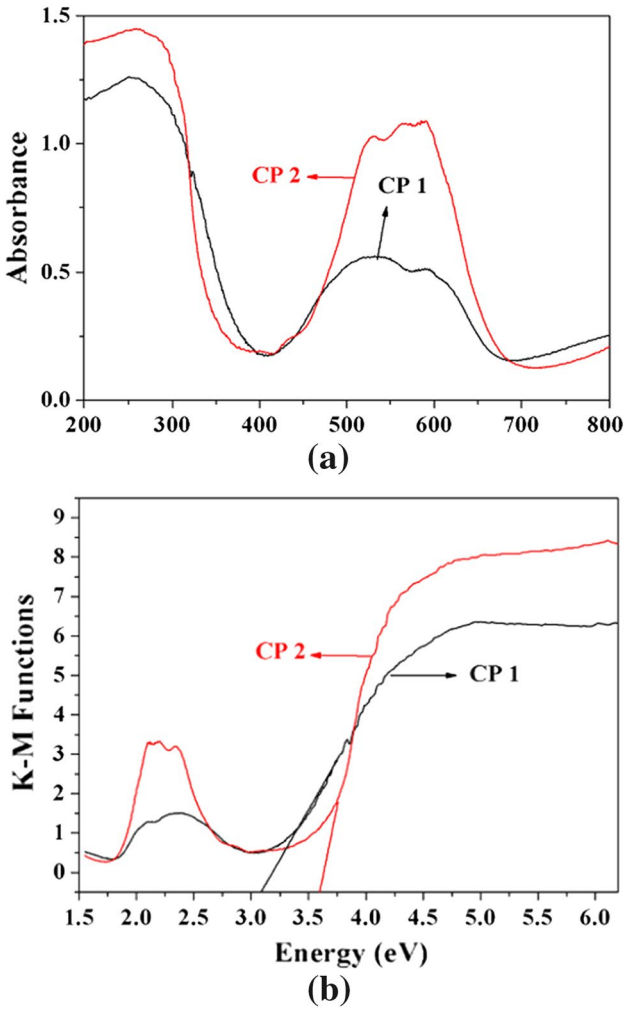

Fig. 5 **a** UV/Vis absorption spectra of CPs **1**–**2** with $BaSO_4$ as background. **b** Diffuse reflectance spectra of Kubelka–Munk function versus energy of CPs **1**–**2**

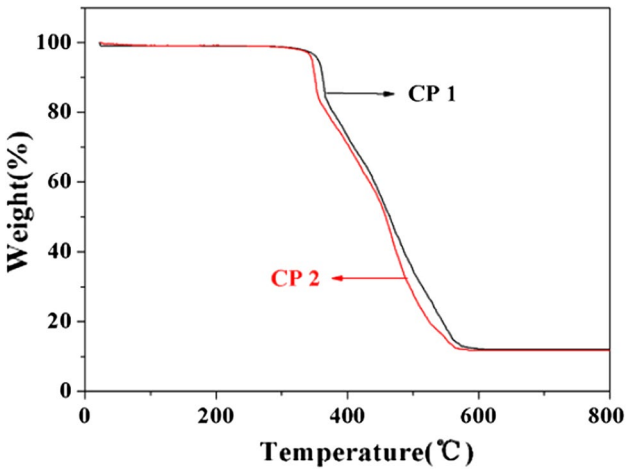

Fig. 6 TG curves of CPs **1**–**2**

Photocatalytic properties

In this work, the organic dye MB was selected as a target pollutant in order to study the photocatalytic properties of CPs **1** and **2**. The change in concentration of MB was followed by the characteristic absorption bond at 664 nm (Fig. 7). The absorption peak did not show any significant change when the solution was kept in the dark. However, the absorption bands of MB decreased with increasing time of irradiation from 0 to 120 min in the presence of both photocatalysts CP **1** and CP **2**. The degradation efficiency for MB reached nearly 86.6% for CP **1** and 83.1% for CP **2** after 120 min, while the degradation efficiency of a blank experiment without photocatalyst was 22.2% after 120 min under the same conditions. Hence, both CPs are effective photocatalysts for the degradation of MB, with very similar performances.

Conclusion

Two Co(II) coordination polymers, $[Co(L1)(DCTP)]_n$ and $[Co(L2)(DCTP)]_n$ based on $DCTP^{2-}$ and different N-donor ligands were synthesized under hydrothermal conditions. CP 1 shows a 2D double-layer structure, while CP 2 exhibits a 3D supramolecular framework involving C–H···O hydrogen bond interactions. These results demonstrate that the spacer length of flexible bis(5,6-dimethylbenzimidazole) ligands plays an important role in construction of coordination polymers with diverse structural features. Both CPs displayed high photocatalytic activity for the degradation of MB.

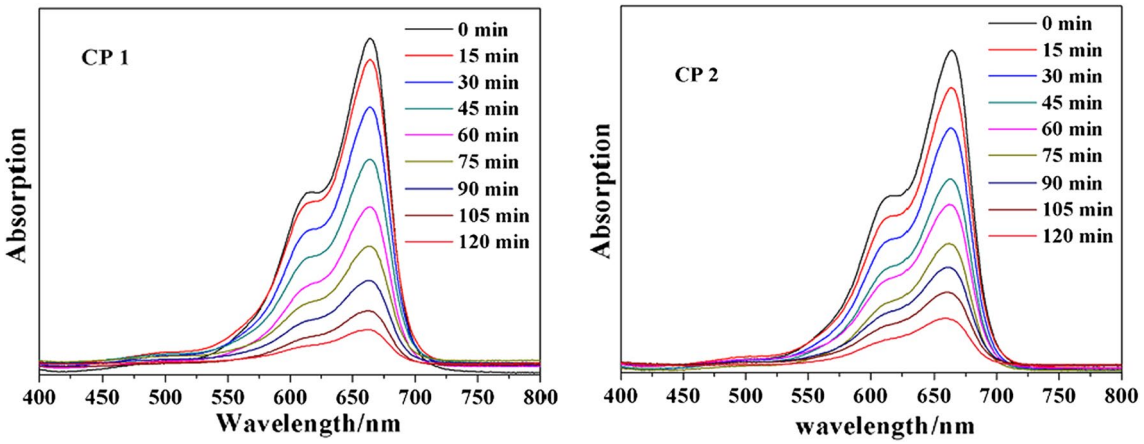

Fig. 7 Absorption spectra of the MB solution during the decomposition reaction under UV irradiation with the presence of photocatalysts CPs **1**–**2**(left for CP **1**, right for CP **2**)

Supplementary material

CCDC 1565136 and 1565137 contain the supplementary crystallographic data for the CPs **1–2**. These data can be obtained free of charge via http://www.ccdc.cam.ac.uk/conts/retrieving.html, or from the Cambridge Crystallographic Data Centre, 12 Union Road, Cambridge CB2 1EZ, UK; fax: (+44) 1223-336-033; or e-mail: deposit@ccdc.cam.ac.uk.

Acknowledgments The work was supported by the National Natural Science Foundation of China (51474086), Natural Science Foundation—Steel and Iron Foundation of Hebei Province (B2015209299).

References

1. Hu JM, Blatov VA, Yu BY, Van Hecke K, Cui GH (2016) Dalton Trans 45:2426–2429
2. Van de Voorde B, Bueken B, Denayer J, De Vos D (2014) Chem Soc Rev 43(16):5766–5788
3. Liu J, Chen L, Cui H, Zhang J, Zhang L, Su CY (2014) Chem Soc Rev 43(16):6011–6061
4. Cui JW, Hou SX, Van Hecke K, Cui GH (2017) Dalton Trans 46:2892–2903
5. McKinlay AC, Eubank JF, Wuttke S, Xiao B, Wheatley PS, Bazin P, Lavalley JC, Daturi M, Vimont A, De Weireld G, Horcajada P, Serre C, Morris RE (2013) Chem Mater 25(9):1592–1599
6. Dhakshinamoorthy A, Asiri AM, Garcia H (2014) Chem Commun 50(85):12800–12814
7. Wang XX, Yu B, Van Hecke K, Cui GH (2014) RSC Adv 4(106):61281–61289
8. Fang DL, Mo SY, Wu KF, Huang ZJ (2017) Transit Met Chem 42:273–283
9. Li SL, Lan YQ, Ma JF, Yang J, Wei GH, Zhang LP, Su ZM (2008) Cryst Growth Des 8(2):675–684
10. Liu J, Zhang HB, Tan YX, Wang F, Kang Y, Zhang J (2014) Inorg Chem 53(3):1500–1506
11. Zhu X, Sun PP, Ding JG, Li BL, Li HY (2012) Crystal Growth Des 12:3992–3997
12. Wang DZ, Li JP, Fan JZ, Jia DZ (2016) Polyhedron 111:123–131
13. Hao SY, Li YF, Li YH, Cui GH (2017) Polyhedron 133:169–178
14. Deria P, Mondloch JE, Karagiaridi O, Bury W, Hupp JT, Farha OK (2014) Chem Soc Rev 43(16):5896–5912
15. Hao SY, Hao ZC, Liu YG, Dong GY (2017) Chin J Struct Chem 36(1):118–126
16. Du DY, Qin JS, Li SL, Su ZM, Lan YQ (2014) Chem Soc Rev 43(13):4615–4632
17. Qin L, Xiao SL, Ma PJ, Cui GH (2013) Transit Metal Chem 38(6):627–633
18. Li CP, Chen J, Mu YH, Du M (2015) Dalton Trans 44(24):11109–11118
19. Guo XG, Yang WB, Wu XY, Zhang QK, Lu CZ (2013) CrystEngComm 15(46):10107
20. Liu GX, Zhu K, Xu HM, Nishihara S, Huang RY, Ren XM (2010) CrystEngComm 12:1175–1185
21. Dong YM, Fan RQ, Wang XM, Wang P, Zhang HJ, Wei LG, Chen W, Yang YL (2016) Cryst Growth Des 16:3366–3378
22. Zhang DP, Bian YZ, Qin J, Wang P, Chen X (2014) Dalton Trans 43:945–949
23. Wang XL, Sha XT, Liu GG, Chen NL, Tian Y (2015) CrystEngComm 17:7290–7299
24. Liu L, Ding J, Li M, Lv X, Wu J, Hou H, Fan Y (2014) Dalton Trans 43:12790–12799
25. Hao SY, Li YH, Hao ZC, Cui GH (2017) Ultrason Sonochem 37:414–423
26. Carter KP, Kalaj M, Cahill CL (2017) Inorg Chem Frontiers 4(1):65–78
27. Fairley TA, Tidwell RR, Donkor I, Naiman NA, Ohemeng KA, Lombardy RJ, Bentley JA, Cory M (1993) J Med Chem 36:1746–1753
28. Sheldrick GM (2015) Acta Crystallogr Sect A 71:3–8
29. Yang L, Powell DR, Houser RP (2007) Dalton Trans 0(9):955–964
30. Meng XM, Fan CB, Bi CF, Zong ZA, Zhang X, Fan YH (2016) CrystEngComm 18(16):2901–2912
31. Ganesan P, Ranganathan R, Chi Y, Liu XK, Lee CS, Liu SH, Lee GH, Lin TC, Chen YT, Chou PT (2017) Chem-Eur J 23(12):2858–2866
32. Dai M, Su XR, Wang X, Wu B, Ren ZG, Zhou X, Lang JP (2014) Cryst Growth Des 14:240–248
33. Liu L, Ding J, Huang C, Li M, Hou HW, Fan YT (2014) Cryst Growth Des 14:3035–3043